ELSEVIER

Contents lists available at ScienceDirect

Journal of Crystal Growth

journal homepage: www.elsevier.com/locate/jcrysgro



Self-assembly of tensile-strained Ge quantum dots on InAlAs(111)A



Kathryn E. Sautter^{a,*}, Christopher F. Schuck^a, Trent A. Garrett^b, Ariel E. Weltner^a, Kevin D. Vallejo^a, Dingkun Ren^c, Baolai Liang^d, Kevin A. Grossklaus^e, Thomas E. Vandervelde^e, Paul J. Simmonds^{a,b,*}

- ^a Micron School of Materials Science & Engineering, Boise State University, Boise, ID, 83725 USA
- ^b Department of Physics, Boise State University, Boise, ID, 83725 USA
- ^c Department of Electrical Engineering, University of California, Los Angeles, CA 90095 USA
- ^d California NanoSystems Institute, University of California, Los Angeles, CA 90095 USA
- ^e Department of Electrical and Computer Engineering, Tufts University, Medford, MA 02155 USA

ARTICLE INFO

Communicated by R. M. Biefeld

Keywords:
Tensile
Self-assembly
Strain
Engineering
Quantum
Dots
Non-traditional
Surface
(111)

ABSTRACT

A recently developed growth technique enables the self-assembly of defect-free quantum dots on (111) surfaces under large tensile strains. We demonstrate the use of this approach to synthesize germanium (Ge) quantum dots on $In_{0.52}Al_{0.48}As(111)A$ with >3% residual tensile strain. We show that the size and areal density of the tensile-strained Ge quantum dots are readily tunable with growth conditions. We also present evidence for an unusual transition in the quantum dot growth mode from Stranski-Krastanov to Volmer-Weber as we adjust the substrate temperature. This work positions Ge quantum dots as a promising starting point for exploring the effects of tensile strain on Ge's band structure.

1. Introduction

Tunable

Germanium (Ge) is an indirect band gap semiconductor that plays a pivotal role in today's electronics industry. However, theory predicts that tensile strain should cause dramatic changes to Ge's band structure, opening up new possibilities for electronic and optoelectronic applications [1–6]. Of particular note is the prediction that for Ge with a (111) crystallographic orientation, ~4% biaxial tensile strain should shrink the band gap to zero, transforming Ge from a semiconductor into a semimetal [2,5-7]. Highquality semiconductor materials with a (111) crystallographic orientation are growing in demand, offering unique characteristics that are highly relevant to a range of applications from quantum optics to topological insulators [8-11]. Transforming the fundamental properties of a material as widely used as Ge would be in and of itself interesting. However, the ability to create functionalized (111)-oriented heterostructures by embedding semimetallic materials within semiconductor matrices could be useful in areas ranging from solar cells to thermoelectrics [12-14]. Zero band gap Ge could even have implications for future topological materials based on conventional semiconductors [15].

As a result of these predictions, researchers have hence explored various approaches to induce tensile strain in Ge, ranging from mechanical stress, to self-assembled Ge nanostructures [16–22]. As a result, tensile strains as large as 3.8% have been achieved in Ge, leading to the observation of some of the predicted changes in band structure [20]. However, these activities have been almost exclusively limited to (001)-oriented Ge, such that tensile-strained Ge with a (111) orientation remains unexplored. To facilitate research in this area, what is first required is a robust method by which we can synthesize defect-free Ge under large tensile strains on (111)-oriented substrates.

In recent years, tensile-strained self-assembly has been established as a scalable, one-step technique for the growth of tensile-strained quantum dots (TSQDs) by molecular beam epitaxy (MBE) [23–25]. The specific combination of tensile strain and a (111) or (110) surface orientation creates an energetic barrier to plastic strain relief by dislocation nucleation and glide [23,25,26]. As a result, a window exists within which elastic strain relief by the self-assembly of dislocation-free 3D islands (TSQDs) can take place. This situation is analogous to the well-known self-assembly of compressively strained QDs on (001)

E-mail addresses: katiesautter@boisestate.edu (K.E. Sautter), paulsimmonds@boisestate.edu (P.J. Simmonds).

^{*} Corresponding author.

surfaces [27–29]. We have previously used this process to synthesize defect-free GaAs TSQDs under 3.7% tensile strain on $In_{0.52}Al_{0.48}As(111)$ and (110) surfaces [8,26,30–32]. These GaAs TSQDs are optically active, with properties that are readily tunable with MBE growth parameters [8,26,30,31,33].

In this paper, we adapt tensile-strained self-assembly to enable the growth of defect-free Ge nanostructures on InAlAs(111)A. Crucially, the model for tensile-strained self-assembly is expected to apply to both zinc-blende (e.g., GaAs) and diamond-cubic (e.g., Ge) semiconductors [25]. Since GaAs and Ge have similar lattice constants, substituting Ge for GaAs in the InAlAs-based material system described above should be a direct replacement, at least from the point of view of the tensile strain. We discuss the role that the MBE growth parameters play in controlling the size and areal density of the Ge TSQDs. We also present evidence for a rarely observed transition between the Stranski-Krastanov (SK) and Volmer-Weber (VW) growth modes for TSQD self-assembly with increasing substrate temperature. Robust control over TSQD synthesis establishes these nanostructures as a useful basis for future studies of tensile-strain-engineered Ge.

2. Methodology

We used solid-source MBE to grow several series of Ge/ $In_{0.52}Al_{0.48}As/InP(111)A$ samples under different growth conditions. The InP(111)A substrates were Fe-doped and nominally on-axis (\pm 0.5°). We used standard effusion cells for the ultra-high purity Al, Ga, In, and Ge, and a valved-source for the As_4 with the cracker set to 600 °C. We determined the substrate temperature (T_{SUB}) with a pyrometer and a thermocouple calibrated against known changes in surface reconstruction, observed with reflection high-energy electron diffraction (RHEED). We used a flux monitor to measure the beam equivalent pressure (BEP) for each source at the substrate position.

We found the Al, Ga, and In growth rates using RHEED intensity oscillations, and calibrated ternary alloy compositions using *ex situ* x-ray diffraction. We calibrated Ge growth rate using transmission electron microscopy (TEM) to measure the thicknesses of Ge layers grown for one hour at different cell temperatures.

For sample growth, we removed the substrate surface oxide by heating in the growth chamber at $T_{SUB}=510~^{\circ}\text{C}$ for 15 min under an As $_4$ BEP of 1.5×10^{-5} Torr. We reduced T_{SUB} to 495 $^{\circ}\text{C}$ and grew a 50 nm $In_{0.53}Ga_{0.47}As$ (hereafter InGaAs) smoothing layer [34], followed by a 200 nm $In_{0.52}Al_{0.48}As$ (hereafter InAlAs) bottom barrier, at growth rates of 169 nm/hr. and 175 nm/hr., respectively. We adjusted T_{SUB} to 435–560 $^{\circ}\text{C}$, closed the As $_4$ valve and shutter, waited for 60 s, and deposited 0.2–1.2 bilayers (BL) of Ge at growth rates from 0.010 to 0.025 BL/s. We then either immediately cooled the Ge layer or buried it with a 20 nm InAlAs top barrier, finishing with a 5 nm InGaAs cap to prevent oxidation.

For each T_{SUB} value of 435, 460, 485, 510, 535, and 560 °C, we grew samples with 0.2, 0.4, 0.6 and 1.2 BL of Ge at 0.020 BL/s, to create a 6 \times 4 sample matrix. We also grew two additional samples with 0.9 BL Ge at 435 °C and 460 °C to add detail in key areas.

From atomic force microscopy (AFM) scans, we extracted the root-mean-square roughness ($\rm R_q$) of the uncapped Ge, as well as the heights, diameters, and areal densities of any nanostructures. We mapped the crystal and compositional structure of our samples using scanning TEM (STEM) with electron energy loss spectroscopy (EELS) and energy-dispersive x-ray spectrometry (EDS). We used ImageJ and NanoScope software to analyze EELS maps and AFM images respectively. To measure residual tensile strain in the Ge TSQDs using Raman spectroscopy, we grew a sample at 535 °C containing four layers of 0.6 BL TSQDs separated by 20 nm InAlAs barriers. Taking care to minimize sample heating, we compared Raman spectra from this four-layer Ge/InAlAs TSQD sample to those from two bulk InAlAs(111)A control samples: one uncapped, and one with a 10 nm InGaAs cap.

3. Results & Discussion

TSQDs form spontaneously when Ge is deposited onto InAlAs (111)A. Prior to Ge deposition, the InAlAs(111)A buffer surfaces (i.e. 0 BL Ge) are smooth, with monolayer-high steps and $R_{\rm q}=0.28$ nm (Fig. 1(a)). Once we start to deposit Ge at $T_{\rm SUB}=535\,^{\circ}{\rm C}$, the surface morphology changes abruptly. Upon opening the Ge shutter, the (2 \times 2) InAlAs(111)A RHEED pattern changes to (1 \times 1), followed rapidly by the appearance of a bright spotty pattern. AFM reveals 3D Ge TSQDs distributed across the surface, with average height 1.81 \pm 0.39 nm (Fig. 1(b)). Analysis of AFM images such as Fig. 1(b) shows that more than 80% of Ge TSQDs nucleate at step edges as opposed to on the terraces. As we raise the Ge deposition amount to 0.6 BL, $R_{\rm q}$ increases from 0.32 nm to 0.51 nm (Fig. 1(c)), accompanied by an increase in the areal density and size of the Ge TSQDs, with average height 2.21 \pm 0.54 nm (Fig. 1(b–c)).

High-resolution TEM imaging, combined with STEM/EELS compositional mapping, confirms the presence of discrete, dislocation-free Ge TSQDs embedded within the InAlAs matrix (Fig. 2(a–b)). A survey of multiple Ge TSQDs suggests that 80–85% are dislocation-free, and hence coherently tensile-strained to the InAlAs (Supplementary Data Fig. S1). We do see some evidence of defects in regions of the InAlAs cap, including triple-period ordering, dislocations, twinning, and

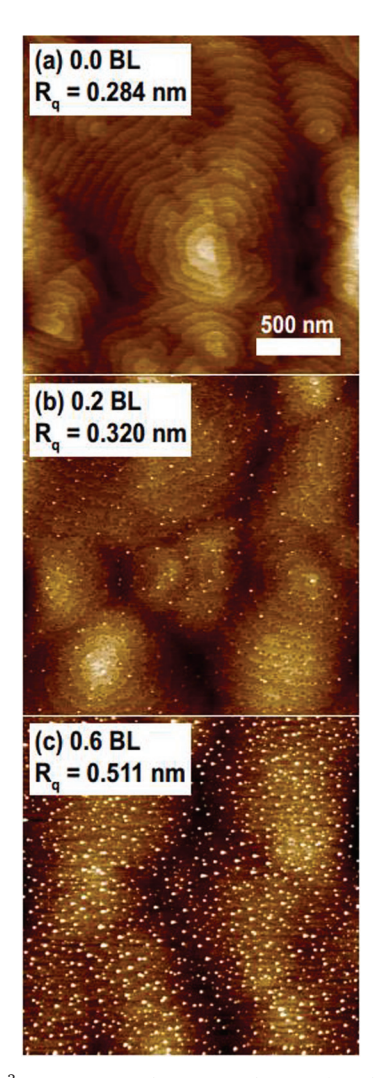


Fig 1. $2\times 2~\mu m^2$ AFM images showing evolution of InAlAs(111)A surface morphology and RMS roughness (R_q) with increasing Ge deposition: (a) 0 BL Ge (i.e. InAlAs(111)A buffer), (b) 0.2 BL Ge, and (c) 0.6 BL Ge. Ge deposition rate = 0.020 BL/s, and $T_{SUB}=535~^{\circ}$ C. The z-scalebar is 2 nm.

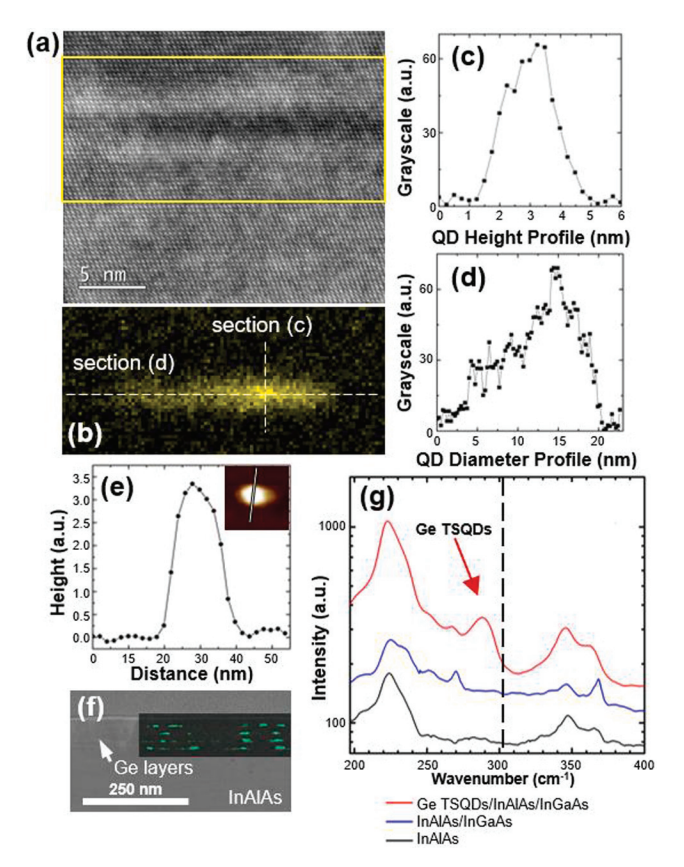


Fig. 2. (a) Annular dark field STEM image of an individual, capped Ge TSQD. (b) an EELS map of the Ge L signal corresponding to the region enclosed by the yellow box in (a). (c) and (d): grayscale profiles showing TSQD height (c) and diameter (d) cross-sections along the dashed lines on the EELS map in (b). (e) AFM cross-section of a representative Ge TSQD on an InAlAs surface (Inset: the 50 nm \times 50 nm AFM image of the TSQD shows the location of the cross-sectional profile (z-scalebar = 4.3 nm)). (f) TEM image overlaid with an EDS elemental map of the Ge K α 1 line. (g) Raman spectra of bulk InAlAs(111)A containing Ge TSQD layers and capped with InGaAs (blue), and InAlAs(111)A containing Ge TSQD layers and capped with InGaAs (red). The black dashed line shows the position of the LO phonon line for unstrained, bulk Ge(111). All samples in this figure were grown with 0.6 BL Ge at 535 °C, with a growth rate of 0.020 BL/s.

stacking faults. However, unlike growth of III-Vs on (001)-oriented Ge, we do not see antiphase domains at the non-polar/polar interface [35,36]. Atomic steps that are an odd number of atomic layers high are energetically very unfavorable on a (111) surface, and so antiphase domains are not expected to form [37]. Future work will focus on optimizing nucleation of the InAlAs above the Ge TSQDs.

The EELS maps in Fig. 2(b) and Fig. S1 reveal no sign of a Ge wetting layer beneath the TSQD. Diffusion of the Ge from the TSQDs into the surrounding InAlAs also appears to be negligible. Taking profiles through the EELS map in Fig. 2(b), we determine a TSQD height of 3.2 \pm 0.4 nm and diameter of 16.7 \pm 1.0 nm (Figs. 2(c,d)). These values are similar to AFM profiles of representative uncapped TSQDs (Fig. 2 (This needs to be linked with Fig. 2e)): height = 3.4 \pm 0.3 nm; diameter = 18 \pm 1 nm. These results suggest minimal alloying of the Ge TSQDs with the surrounding InAlAs matrix.

Fig. 2(f) shows a TEM image of a sample containing four stacked layers of Ge TSQDs. Consistent with EELS, an EDS elemental map (Fig. 2(f) inset) shows discrete Ge TSQDs. EDS also reveals vertical alignment of the Ge TSQDs in consecutive layers. The tensile strain field surrounding each Ge TSQD enhances the probability of another TSQD nucleating directly above it in the next layer, a well-known effect in compressively strained QD systems [38]. This observation provides additional confirmation that the Ge TSQDs are coherently tensile-strained to the InAlAs matrix.

To quantify the amount of tensile strain within the Ge TSQDs, Fig. 2(g) compares the Raman spectrum from the sample in Fig. 2(f) with those from InAlAs control samples. The InAs phonon lines at 220 cm $^{-1}$ (TO₁) and 237 cm $^{-1}$ (LO₁), and the AlAs phonon lines at 347 cm $^{-1}$ (TO₂) and 369 cm $^{-1}$ (LO₂), are common to the Raman spectra from all samples (Fig. 2(g)) [39]. The samples containing In-GaAs also show InAs-like LO and GaAs-like TO lines at 251 cm⁻¹ and 268 cm⁻¹ respectively [40]. Unique to the Ge TSQD Raman spectrum is the feature at 288.4 cm⁻¹, corresponding to the LO phonon line of the Ge TSODs. This line is shifted from 302.4 cm⁻¹ where we observe the LO phonon for bulk, unstrained Ge(111) (dashed line). From this Raman shift of -14.0 cm⁻¹, we calculate the tensile strain in the Ge TSQDs to be 3.38 \pm 0.36% using a value of -415 \pm 40 cm⁻¹ for the phonon strain-shift coefficient [41]. Although this calculated tensile strain is a little lower than the 3.7% lattice mismatch between Ge and In_{0.52}Al_{0.48}As, they agree within error. The most likely causes of any discrepancy are elastic strain relief in the Ge TSQDs, and typical run-torun variations in the composition of the InAlAs layers used in the Raman sample. The asymmetric broadening of the Ge TSQD line towards lower wavenumbers (Fig. 2(g)) is observed in the Raman spectra of other QD systems, including strain-free Ge QDs, and compressively strained InAs QDs [21,42]. These asymmetric phonon line shapes derive from optical phonon confinement in arrays of QDs with a finite size distribution [43-45].

We can readily tune TSQD size and areal density by controlling T_{SUB} and Ge deposition during MBE growth. In the interest of space, Fig. 3 shows only a subset of the full sample matrix. Each row shows the effect of raising T_{SUB} , while each column shows the effect of increasing Ge deposition. To avoid thermal degradation of the InAlAs, we were limited to $T_{SUB} \, < \, 560 \, ^{\circ}\text{C}$.

Surprisingly, Fig. 3 reveals that there are two growth modes responsible for Ge TSQD self-assembly in this sample set. At $T_{SUB} = 435$ °C, there is no TSQD formation for ≤ 0.6 BL Ge (Fig. 3(a), (e)), indicating that Ge initially grows as a 2D wetting layer. However, for deposition ≥ 0.9 BL, the Ge self-assembles into 3D TSQDs (Fig. 3(i)). This 2D-to-3D growth transition is consistent with the SK growth mode. Barabási suggests that there are two kinds of SK growth depending on whether growth is thermodynamically or kinetically limited [46]. The far-from-equilibrium nature of MBE means we observe the kinetically limited version of SK growth here. As T_{SUB} is increased to 485 °C, we again see TSQD self-assembly via the SK mode with a transition from 2D growth (Fig. 3(b)) to 3D growth (Fig. 3(f)) as deposition is increased. Interestingly, the critical thickness of 0.6 BL for the 2D-to-3D SK transition is lower than at 435 °C. This observation is consistent with previous studies, which showed reduced SK critical thickness for increased adatom diffusion length:[47-49] in our case, by increasing T_{SUB}. From the areal density and average TSQD volume, we calculate that in Fig. 3(f) only 0.61 \pm 0.24% of the total 0.6 BL Ge deposited is contained within the TSQDs, with the remainder in the wetting layer. We therefore estimate the wetting layer is $\sim\!0.596~BL$ thick, and since this value is greater than 0.5 BL (i.e. 1 monolayer), we conclude that the wetting layer is continuous over the surface, consistent with SK growth.

In contrast, for $T_{SUB} \geq 510$ °C, we see TSQD formation after deposition of just 0.2 BL Ge (Fig. 3(c,d)), which is insufficient for a continuous wetting layer to form. Immediate TSQD self-assembly in the absence of a wetting layer indicates that for $T_{SUB} \geq 510$ °C, growth proceeds via the VW mode. Indeed, both EELS and EDS in different samples grown at $T_{SUB} = 535$ °C confirm the absence of a continuous Ge wetting layer (Fig. 2 and Fig. S1).

The ability to controllably change the growth mode from SK to VW is very unusual. Although theory predicts that a transition between SK and VW growth modes is possible [46], experimental evidence is scarce. We have previously seen hints of a crossover from SK to VW growth during GaAs TSQD self-assembly [26]. Other researchers have used substrate offcut angle to move from SK to VW self-assembly during

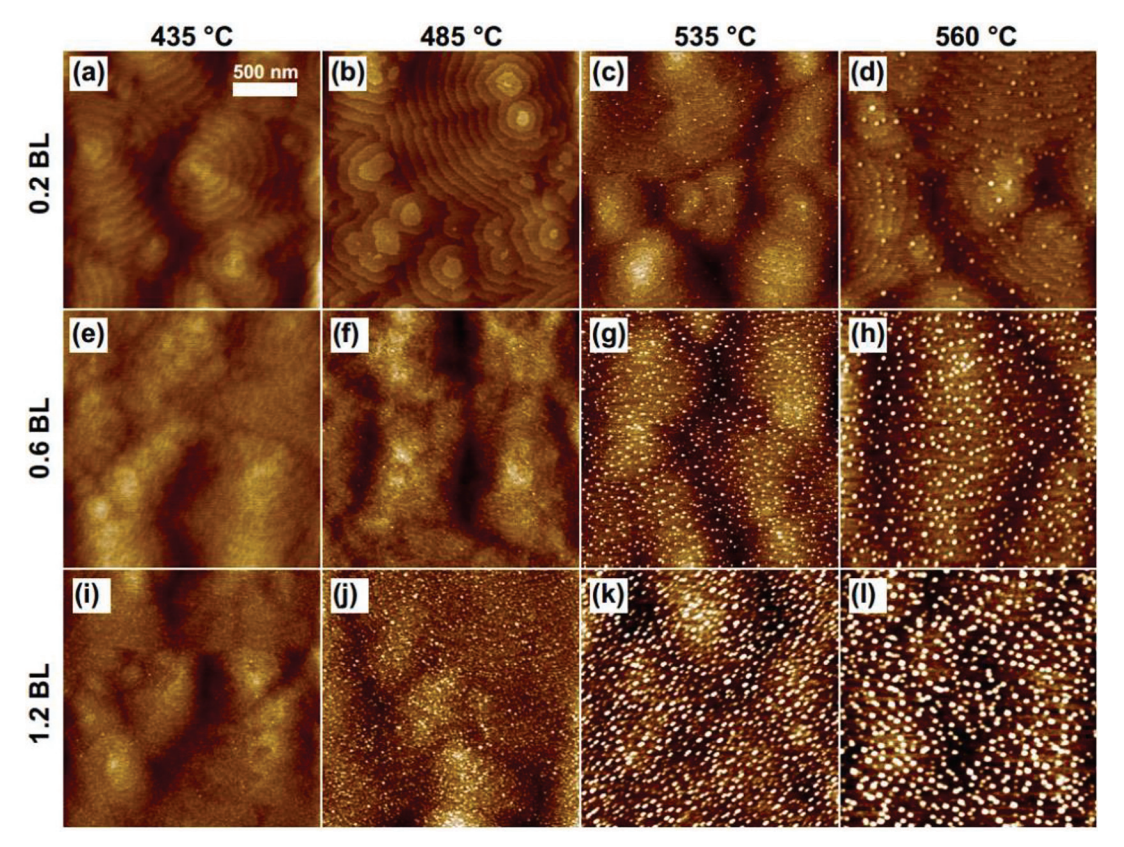


Fig. 3. $2 \times 2 \,\mu\text{m}^2$ AFM images demonstrating control of Ge TSQD size and density as a function of both Ge deposition amount (rows) and T_{SUB} (columns). All samples were grown at 0.020 BL/s. The z-scalebar is 2 nm.

growth of GeSi on Si(001), which is a function of surface free energy variations in the facets available at different angles [50–52].

Whether self-assembly occurs via the SK or VW growth modes is due to the interplay between the strain and free surface energies of a particular QD material system [53]. For the Ge/InAlAs(111)A TSQD system, the tensile strain and surface energies of the InAlAs buffer and the Ge/InAlAs interface are constant regardless of T_{SUB} . It is therefore likely that, consistent with the case for offcut substrates [50], the observed SK-to-VW transition is linked to the higher surface free energy of Ge crystal facets that become accessible when T_{SUB} increases [54]. Although outside the scope of the work presented here, a future study using scanning tunneling microscopy will help clarify this point.

Fig. 3 also provides some insight into the surface diffusivity of Ge adatoms on InAlAs(111)A. The fact that greater than 80% of TSQDs form at step edges on the InAlAs(111)A surface (e.g. Fig. 1(b), Fig. 3(c,d)) is often taken as a signature of a high adatom diffusion length [25]. The average InAlAs(111)A terrace width is 86 ± 13 nm, so to reach the nearest step edge, the average Ge adatom must diffuse a distance \geq 43 \pm 7 nm. However, we expect Ge adatom diffusion lengths to be greater than 50 nm. On Si(001) surfaces, Ge adatoms diffuse more than 2 µm [55], a value that should be even higher on (111) surfaces that are known to have longer diffusion lengths than (001) surfaces [56].

We therefore conclude that the Ehrlich-Schwöbel (ES) barrier limiting adatom migration between neighboring terraces of the InAlAs (111)A surface must be larger than the kinetic energy of the Ge adatoms over the range of T_{SUB} used here. Although values for the ES barrier on InAlAs(111)A are unavailable in the literature, it is known that ES barriers on (111)A surfaces of III-V compounds are typically large. A previous study estimated an ES barrier for Ga(Al)As(111)A of at least 100 meV [57]. We hence attribute the preferential nucleation of Ge/InAlAs(111)A TSQDs at step edges to a large ES barrier limiting Ge adatom diffusion.

2D contour plots of structural data from our 6 \times 4 sample matrix reveal a local maximum in TSQD areal density for 0.6 BL Ge grown at $T_{SUB} = 510\text{--}535\,^{\circ}\text{C}$ (Fig. 4(a)). The local maximum for TSQD height occurs for 0.6 BL Ge grown at $T_{SUB} = 535\,^{\circ}\text{C}$ (Fig. 4(b)). As expected for mass conservation, we see a corresponding local minimum in TSQD diameter for 0.6 BL Ge grown at 510–535 $^{\circ}\text{C}$ (Fig. 4(c)). If high-density, tall, narrow TSQDs are desirable, these growth conditions should be targeted. The maximum areal density of 4.44 \times 10¹⁰ cm⁻² occurs for 1.2 BL Ge TSQDs grown at 510 $^{\circ}\text{C}$.

At the highest values of T_{SUB} and deposition (upper righthand corners in Fig. 4), there is a decrease in TSQD areal density, accompanied by a sharp increase in TSQD height and diameter to their maximum values over the range studied here. This behavior corresponds to Ostwald ripening of the TSQDs [58]. Raising T_{SUB} increases the Ge adatom diffusion length, allowing bigger TSQDs to grow at the expense of smaller ones nearby. This results in a lower density of larger Ge TSQDs that minimize the strain energy more efficiently than numerous small TSQDs.

We can also tailor TSQD self-assembly via the Ge growth rate. Holding total Ge deposition constant at 0.6 BL, we raised the Ge growth rate from 0.010 to 0.025 BL/s (Supplementary Data Fig. S2). TSQD areal density increases from 5.3 to $19.0\times10^9~\rm cm^{-2}$, with a simultaneous decrease in average TSQD diameter from 29.5 \pm 4.3 to 23.1 \pm 0.9 nm, and a small increase in average height from 1.84 \pm 0.46 to 2.59 \pm 0.40 nm. Since adatom diffusion length decreases at higher growth rates, adatoms tend to cluster closer to where they land on the surface [25,59]. The result is a higher density of smaller dots

The dependences of Ge TSQD size and areal density on the three MBE parameters explored here (T_{SUB} , deposition amount, and growth rate) are consistent with the self-assembly behavior of III-V QDs: both traditional compressively strained (001) QDs and tensile-strained QDs on (110) and (111) surfaces [23–25,53]. These similarities indicate that

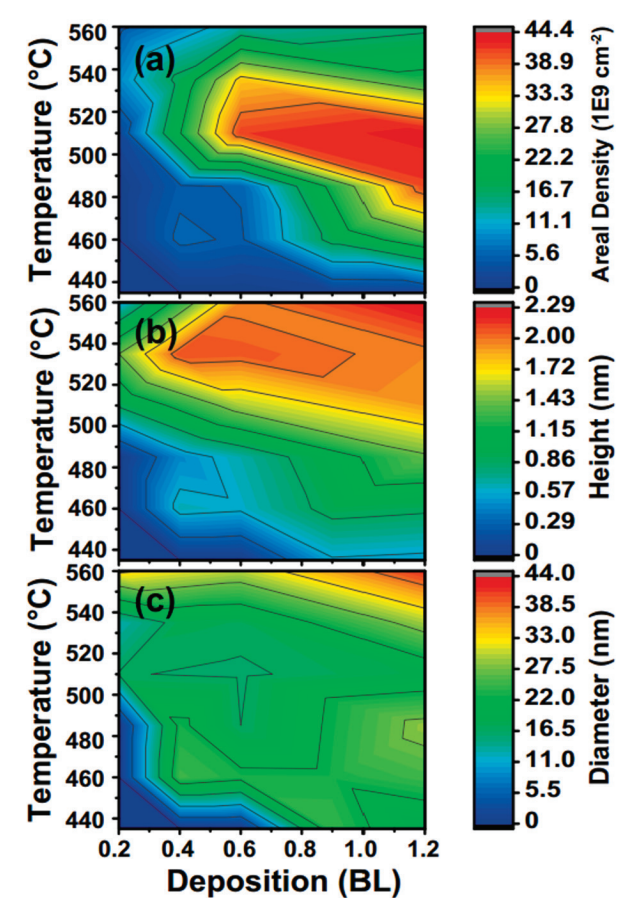


Fig. 4. Contour plots summarizing changes in TSQD (a) areal density, (b) height, and (c) diameter as a function of Ge deposition amount and $T_{\rm SUB}.$

despite the introduction of Ge, a group IV semiconductor, the same physical processes underpin self-assembly. We can therefore apply the extensive body of knowledge surrounding III-V QDs to hybrid group IV/ III-V QD systems like this as we begin to develop them for specific applications.

4. Conclusions

We demonstrate the controllable growth of self-assembled Ge TSQDs on InAlAs(111)A. We can readily tune TSQD size and areal density in response to T_{SUB}, deposition amount, and growth rate. With Raman spectroscopy, we measure residual strains in the Ge TSQDs of 3.4% and observe indications of optical phonon confinement. We see compelling evidence for an unusual transition between the SK and VW growth modes for TSQD self-assembly. Self-assembly of Ge/InAlAs (111)A TSQDs provides the clearest evidence to date for a tunable transition between the SK and VW growth modes. The ability to select either the SK or VW growth mode for QD self-assembly, simply by controlling T_{SUB}, could be useful for certain applications. Its near ubiquity in III-V QD self-assembly means SK growth is very well-understood. On the other hand, VW growth eliminates the possibility of QDwetting layer interactions [60], while the lack of a wetting layer could help minimize antiphase disorder when capping Ge TSQDs with a III-V top barrier [21]. This work represents a robust starting point from which to use tensile-strained band engineering to investigate the transformation of Ge into a semimetal or direct band gap semiconductor [6,7].

Declaration of Competing Interest

The authors declare that they have no known competing financial interests or personal relationships that could have appeared to influence the work reported in this paper.

Acknowledgements

This material is based upon work supported by the Air Force Office of Scientific Research under award number FA9550-16-1-0278.

Appendix A. Supplementary material

Supplementary data to this article can be found online at https://doi.org/10.1016/j.jcrysgro.2019.125468.

References

- M. El Kurdi, G. Fishman, S. Sauvage, P. Boucaud, Band structure and optical gain of tensile-strained germanium based on a 30 band k-p formalism, J. Appl. Phys. 107 (2010) 013710, https://doi.org/10.1063/1.3279307.
- [2] O. Aldaghri, Z. Ikonić, R.W. Kelsall, Optimum strain configurations for carrier injection in near infrared Ge lasers, J. Appl. Phys. 111 (2012) 053106, https://doi.org/10.1063/1.3691790.
- [3] G.-E. Chang, H.H. Cheng, Optical gain of germanium infrared lasers on different crystal orientations, J. Phys. Appl. Phys. 46 (2013) 065103, https://doi.org/10. 1088/0022-3727/46/6/065103.
- [4] H.S. Lan, S.T. Chan, T.H. Cheng, C.Y. Chen, S.R. Jan, C.W. Liu, Biaxial tensile strain effects on photoluminescence of different orientated Ge wafers, Appl. Phys. Lett. 98 (2011) 101106, https://doi.org/10.1063/1.3562589.
- [5] C.H. Yang, Z.Y. Yu, Y.M. Liu, P.F. Lu, T. Gao, M. Li, S. Manzoor, Dependence of electronic properties of germanium on the in-plane biaxial tensile strains, Phys. B Condens. Matter 427 (2013) 62–67, https://doi.org/10.1016/j.physb.2013.06.015.
- [6] H. Tahini, A. Chroneos, R.W. Grimes, U. Schwingenschlögl, A. Dimoulas, Straininduced changes to the electronic structure of germanium, J. Phys. Condens. Matter 24 (2012) 195802, https://doi.org/10.1088/0953-8984/24/19/195802.
- [7] Y.M. Niquet, D. Rideau, C. Tavernier, H. Jaouen, X. Blase, Onsite matrix elements of the tight-binding Hamiltonian of a strained crystal: Application to silicon, germanium, and their alloys, Phys. Rev. B 79 (2009) 245201, https://doi.org/10.1103/ PhysRevB.79.245201.
- [8] C.D. Yerino, P.J. Simmonds, B. Liang, D. Jung, C. Schneider, S. Unsleber, M.V. Vo, D.L. Huffaker, S. Höfling, M. Kamp, et al., Strain-driven growth of GaAs(111) quantum dots with low fine structure splitting, Appl. Phys. Lett. 105 (2014) 251901, https://doi.org/10.1063/1.4904944.
- [9] X. Guo, Z.J. Xu, H.C. Liu, B. Zhao, X.Q. Dai, H.T. He, J.N. Wang, H.J. Liu, W.K. Ho, M.H. Xie, Single domain Bi2Se3 films grown on InP(111)A by molecular-beam epitaxy, Appl. Phys. Lett. 102 (2013) 151604. https://doi.org/10.1063/1.4802797.
- [10] S.R. Mehrotra, M. Povolotskyi, D.C. Elias, T. Kubis, J.J.M. Law, M.J.W. Rodwell, G. Klimeck, Simulation study of thin-body ballistic N-MOSFETs involving transport in mixed Γ-L valleys, IEEE Electron Device Lett. 34 (9) (2013) 1196–1198, https:// doi.org/10.1109/LED.2013.2273072.
- [11] B.J. May, E.C. Hettiaratchy, R.C. Myers, Controlled nucleation of monolayer MoSe2 islands on Si (111) by MBE, J. Vac. Sci. Technol. B 37 (2019) 021211, https://doi. org/10.1116/1.5087212.
- [12] J.M.O. Zide, A. Kleiman-Schwasctein, N.C. Strandwitz, J.D. Zimmerman, T. Steenblock-Smith, A.C. Gossard, A. Forman, A. Ivanovskaya, G.D. Stucky, Increased efficiency in multijunction solar cells through the incorporation of semimetallic ErAs nanoparticles into the tunnel junction, Appl. Phys. Lett. 88 (2006) 162103, https://doi.org/10.1063/1.2196059.
- [13] A.M. Crook, H.P. Nair, S.R. Bank, High-performance nanoparticle-enhanced tunnel junctions for photonic devices, Phys. Status Solidi C 7 (10) (2010) 2544–2547, https://doi.org/10.1002/pssc.200983914.
- [14] W. Kim, J. Zide, A. Gossard, D. Klenov, S. Stemmer, A. Shakouri, A. Majumdar, Thermal conductivity reduction and thermoelectric figure of merit increase by embedding nanoparticles in crystalline semiconductors, Phys. Rev. Lett. 96 (2006) 045901, https://doi.org/10.1103/PhysRevLett. 96.045901.
- [15] M. Zhao, X. Chen, L. Li, X. Zhang, Driving a GaAs film to a large-gap topological insulator by tensile strain, Sci. Rep. 5 (2015) 8441, https://doi.org/10.1038/ srep08441.
- [16] J. Greil, A. Lugstein, C. Zeiner, G. Strasser, E. Bertagnolli, Tuning the electro-optical properties of germanium nanowires by tensile strain, Nano Lett. 12 (12) (2012) 6230–6234, https://doi.org/10.1021/nl303288g.
- [17] J.R. Sánchez-Pérez, C. Boztug, F. Chen, F.F. Sudradjat, D.M. Paskiewicz, R.B. Jacobson, M.G. Lagally, R. Paiella, Direct-bandgap light-emitting germanium in tensilely strained nanomembranes, Proc. Natl. Acad. Sci. U. S. A. 108 (47) (2011) 18893–18898, https://doi.org/10.1073/pnas.1107968108.

- [18] A. Ghrib, M. El Kurdi, M. de Kersauson, M. Prost, S. Sauvage, X. Checoury, G. Beaudoin, I. Sagnes, P. Boucaud, Tensile-strained germanium microdisks, Appl. Phys. Lett. 102 (2013) 221112, https://doi.org/10.1063/1.4809832.
- [19] Y. Huo, H. Lin, R. Chen, Y. Rong, T.I. Kamins, J.S. Harris, MBE growth of tensile-strained Ge quantum wells and quantum dots, Front. Optoelectron. 5 (1) (2012) 112–116, https://doi.org/10.1007/s12200-012-0193-x.
- [20] D. Jung, J. Faucher, S. Mukherjee, A. Akey, D.J. Ironside, M. Cabral, X. Sang, J. Lebeau, S.R. Bank, T. Buonassisi, O. Moutanabbir, M.L. Lee, Highly tensilestrained Ge/InAlAs nanocomposites, Nat. Commun. 8 (2017) 14204, https://doi. org/10.1038/ncomms14204.
- [21] M. Qi, C.A. Stephenson, V. Protasenko, W.A. O'Brien, A. Mintairov, H. Xing, M.A. Wistey, Ge quantum dots encapsulated by AlAs grown by molecular beam epitaxy on GaAs without extended defects, Appl. Phys. Lett. 104 (2014) 073113, https://doi.org/10.1063/1.4866278.
- [22] Z.P. Zhang, Y.X. Song, Q.M. Chen, X.Y. Wu, Z.Y.S. Zhu, L.Y. Zhang, Y.Y. Li, S.M. Wang, Growth mode of tensile-strained Ge quantum dots grown by molecular beam epitaxy, J. Phys. Appl. Phys. 50 (46) (2017) 465301, https://doi.org/10. 1088/1361-6463/aa8bcf.
- [23] P.J. Simmonds, M.L. Lee, Tensile strained island growth at step-edges on GaAs (110), Appl. Phys. Lett. 97 (2010) 153101, https://doi.org/10.1063/1.3498676.
- [24] P.J. Simmonds, M.L. Lee, Self-assembly on (111)-oriented III-V surfaces, Appl. Phys. Lett. 99 (2011) 123111, https://doi.org/10.1063/1.3640501.
- [25] P.J. Simmonds, M.L. Lee, Tensile-strained growth on low-index GaAs, J. Appl. Phys. 112 (2012) 054313, https://doi.org/10.1063/1.4749407.
- [26] C.F. Schuck, R.A. McCown, A. Hush, A. Mello, S. Roy, J.W. Spinuzzi, B. Liang, D.L. Huffaker, P.J. Simmonds, Self-assembly of (111)-oriented tensile-strained quantum dots by molecular beam epitaxy, J. Vac. Sci. Technol. B 36 (3) (2018) 31803, https://doi.org/10.1116/1.5018002.
- [27] D. Leonard, M. Krishnamurthy, C.M. Reaves, S.P. Denbaars, P.M. Petroff, Direct formation of quantum-sized dots from uniform coherent islands of InGaAs on GaAs surfaces, Appl. Phys. Lett. 63 (23) (1993) 3203–3205, https://doi.org/10.1063/1. 110190
- [28] H.-M. Ji, B. Liang, P.J. Simmonds, B.-C. Juang, T. Yang, R.J. Young, D.L. Huffaker, Hybrid type-I InAs/GaAs and type-II GaSb/GaAs quantum dot structure with enhanced photoluminescence, Appl. Phys. Lett. 106 (2015) 103104, https://doi.org/ 10.1063/1.4914895.
- [29] P.J. Simmonds, R.B. Laghumavarapu, M. Sun, A. Lin, C.J. Reyner, B. Liang, D.L. Huffaker, Structural and optical properties of InAs/AlAsSb quantum dots with GaAs(Sb) cladding layers, Appl. Phys. Lett. 100 (2012) 243108, https://doi.org/10. 1063/1.4729419.
- [30] P.J. Simmonds, C.D. Yerino, M. Sun, B. Liang, D.L. Huffaker, V.G. Dorogan, Y. Mazur, G. Salamo, M.L. Lee, Tuning quantum dot luminescence below the bulk band gap using tensile strain, ACS Nano 7 (6) (2013) 5017–5023, https://doi.org/ 10.1021/np400395v.
- [31] P.J. Simmonds, Quantum Dot Growth on (111) and (110) Surfaces Using Tensile-Strained Self-Assembly, Quantum Dots and Nanostructures: Growth, Characterization, and Modeling XV, 10543 International Society for Optics and Photonics. 2018. p. 1054301. https://doi.org/10.1117/12.2299676.
- Photonics, 2018, p. 105430L, , https://doi.org/10.1117/12.2299676.

 [32] C.D. Yerino, P.J. Simmonds, B. Liang, V.G. Dorogan, M.E. Ware, Y.I. Mazur, D. Jung, D.L. Huffaker, G.J. Salamo, M.L. Lee, Tensile GaAs(111) quantum dashes with tunable luminescence below the bulk bandgap, Appl. Phys. Lett. 105 (2014) 071912, https://doi.org/10.1063/1.4893747.
- [33] C.F. Schuck, S.K. Roy, T. Garrett, Q. Yuan, Y. Wang, C.I. Cabrera, K.A. Grossklaus, T.E. Vandervelde, B. Liang, P.J. Simmonds, Anomalous Stranski-Krastanov growth of (111)-oriented quantum dots with tunable wetting layer thickness, Sci. Rep. 9 (2019) 18179, https://doi.org/10.1038/s41598-019-54668-z.
- [34] C.D. Yerino, B. Liang, D.L. Huffaker, P.J. Simmonds, M.L. Lee, Review article: molecular beam epitaxy of lattice-matched InAlAs and InGaAs layers on InP (111)A, (111)B, and (110), J. Vac. Sci. Technol. B 35 (2017) 10801, https://doi.org/10. 1116/1.4972049.
- [35] R.M. Sieg, S.A. Ringel, S.M. Ting, E.A. Fitzgerald, R.N. Sacks, Anti-phase domain-free growth of GaAs on offcut (001) Ge wafers by molecular beam epitaxy with suppressed Ge outdiffusion, J. Electron. Mater. 27 (7) (1998) 900–907, https://doi.org/10.1007/s11664-998-0116-1.
- [36] T. Masuda, J. Faucher, P.J. Simmonds, K. Okumura, M.L. Lee, Device and material characteristics of GalnP solar cells grown on Ge Substrates by molecular beam epitaxy, In 2016 IEEE 43rd Photovoltaic Specialists Conference, 2016, pp. 2344–2348, https://doi.org/10.1109/PVSC.2016.7750058.
- [37] H. Kroemer, K.J. Polasko, S.C. Wright, On the (110) orientation as the preferred orientation for the molecular beam epitaxial growth of GaAs on Ge, GaP on Si, and similar zincblende-on-diamond systems, Appl. Phys. Lett. 36 (9) (1980) 763–765, https://doi.org/10.1063/1.91643.

- [38] P.J. Simmonds, M. Sun, R.B. Laghumavarapu, B. Liang, A.G. Norman, J.-W. Luo, D.L. Huffaker, Improved quantum dot stacking for intermediate band solar cells using strain compensation, Nanotechnology 25 (44) (2014), https://doi.org/10. 1088/0957-4484/25/44/445402.
- [39] A.G. Milekhin, A.K. Kalagin, A.P. Vasilenko, A.I. Toropov, N.V. Surovtsev, D.R.T. Zahn, Vibrational spectroscopy of InAlAs epitaxial layers, J. Appl. Phys. 104 (2008) 73516, https://doi.org/10.1063/1.2980344.
- [40] H. Kim, H. Rho, E.H. Lee, J.D. Song, Polarized and spatially resolved raman scattering from composition-graded wurtzite InGaAs nanowires, J. Phys. Appl. Phys. 49 (2016) 175105, https://doi.org/10.1088/0022-3727/49/17/175105.
- [41] Y.Y. Fang, J. Tolle, R. Roucka, A.V.G. Chizmeshya, J. Kouvetakis, V.R. D'Costa, J. Menéndez, Perfectly tetragonal, tensile-strained Ge on Ge_{1-y}Sn_y buffered Si(100), Appl. Phys. Lett. 90 (2007) 061915, https://doi.org/10.1063/1.2472273.
- [42] D.A. Tenne, A.K. Bakarov, A.I. Toropov, D.R.T. Zahn, Raman study of self-as-sembled InAs quantum dots embedded in AlAs: Influence of growth temperature, Phys. E Low-Dimens. Syst. Nanostruct. 13 (2–4) (2002) 199–202, https://doi.org/10.1016/S1386-9477(01)00519-7.
- [43] H. Richter, Z.P. Wang, L. Ley, The one phonon raman spectrum in microcrystalline silicon, Solid State Commun. 39 (5) (1981) 625–629, https://doi.org/10.1016/ 0038-1098(81)90337-9.
- [44] A.K. Arora, M. Rajalakshmi, T.R. Ravindran, V. Sivasubramanian, Raman spectroscopy of optical phonon confinement in nanostructured materials, J. Raman Spectrosc. 38 (6) (2007) 604–617, https://doi.org/10.1002/jrs.1684.
- [45] A.G. Rolo, M.I. Vasilevskiy, Raman spectroscopy of optical phonons confined in semiconductor quantum dots and nanocrystals, J. Raman Spectrosc. 38 (6) (2007) 618–633, https://doi.org/10.1002/jrs.1746.
- [46] A.-L. Barabási, Thermodynamic and kinetic mechanisms in self-assembled quantum dot formation, Mater. Sci. Eng. B 67 (1) (1999) 23–30, https://doi.org/10.1016/ S0921-5107(99)00205-6.
- [47] H. Zhang, Y. Chen, G. Zhou, C. Tang, Z. Wang, Wetting layer evolution and its temperature dependence during self-assembly of InAs/GaAs quantum dots, Nanoscale Res. Lett. 7 (2012) 600, https://doi.org/10.1186/1556-276X-7-600.
- [48] A. Riposan, J.M. Millunchick, C. Pearson, Critical film thickness dependence on As flux in In0.27Ga0.73As/GaAs(001) films, Appl. Phys. Lett. 90 (2007) 091902, https://doi.org/10.1063/1.2476259.
- [49] A. Baskaran, P. Smereka, Mechanisms of Stranski-Krastanov growth, J. Appl. Phys. 111 (2012) 044321, https://doi.org/10.1063/1.3679068.
- [50] T. Zhou, Z. Zhong, Dramatically enhanced self-assembly of GeSi quantum dots with superior photoluminescence induced by the substrate misorientation, APL Mater. 2 (2014) 22108, https://doi.org/10.1063/1.4866356.
- [51] B.J. Spencer, J. Tersoff, Asymmetry and shape transitions of epitaxially strained islands on vicinal surfaces, Appl. Phys. Lett. 96 (2010) 073114, https://doi.org/10. 1063/1.3318256.
- [52] L. Persichetti, A. Sgarlata, M. Fanfoni, A. Balzarotti, Shaping Ge islands on Si(001) surfaces with misorientation angle, Phys. Rev. Lett. 104 (2010) 036104, https://doi.org/10.1103/PhysRevLett.104.036104.
- [53] B.A. Joyce, D.D. Vvedensky, Self-organized growth on GaAs surfaces, Mater. Sci. Eng. R Rep. 46 (2004) 127–176, https://doi.org/10.1016/j.mser.2004.10.001.
- [54] I. Daruka, J. Tersoff, A.-L. Barabási, Shape transition in growth of strained islands, Phys. Rev. Lett. 82 (13) (1999) 2753–2756, https://doi.org/10.1103/PhysRevLett. 82 2753
- [55] Y. Jiang, D. Mo, X. Hu, S. Wang, Y. Chen, D. Lin, Y. Fan, X. Yang, Z. Zhong, Z. Jiang, Investigation on Ge surface diffusion via growing Ge quantum dots on top of Si pillars, AIP Adv. 6 (2016) 085120, https://doi.org/10.1063/1.4961992.
- [56] T. Takebe, M. Fujii, T. Yamamoto, K. Fujita, T. Watanabe, Orientation-dependent Ga surface diffusion in molecular beam epitaxy of GaAs on GaAs patterned substrates, J. Appl. Phys. 81 (1997) 7273–7281, https://doi.org/10.1063/1.365548.
- [57] L. Esposito, S. Bietti, A. Fedorov, R. Nötzel, S. Sanguinetti, Ehrlich-Schwöbel effect on the growth dynamics of GaAs(111)A surfaces, Phys. Rev. Mater. 1 (2) (2017) 24602, https://doi.org/10.1103/PhysRevMaterials.1.024602.
- [58] T.J. Krzyzewski, T.S. Jones, Ripening and annealing effects in InAs/GaAs(001) quantum dot formation, J. Appl. Phys. 96 (2004) 668, https://doi.org/10.1063/1.1759788.
- [59] P.B. Joyce, T.J. Krzyzewski, G.R. Bell, T.S. Jones, S. Malik, D. Childs, R. Murray, Effect of growth rate on the size, composition, and optical properties of InAs/GaAs quantum dots grown by molecular-beam epitaxy, Phys. Rev. B 62 (16) (2000) 10891–10895, https://doi.org/10.1103/PhysRevB.62.10891.
- [60] F. Hopfer, A. Mutig, G. Fiol, M. Kuntz, V. Shchukin, N.N. Ledentsov, D. Bimberg, S.S. Mikhrin, I.L. Krestnikov, D.A. Livshits, A.R. Kovsh, C. Bornholdt, et al., 20 Gb/s 85 °C error free operation of VCSEL based on submonolayer deposition of quantum dots, In 2006 IEEE 20th International Semiconductor Laser Conference, IEEE, 2006, pp. 119–120, https://doi.org/10.1109/islc.2006.1708115.